

Anticorrosion Performance of Epoxy Coating Containing Reactive Poly (o-phenylenediamine) Nanoparticles

Cheng Chen^{1,2}, Shihui Qiu², Songlv Qin², Guoping Yan¹, Haichao Zhao^{2,*}, Liping Wang^{2,*}

¹School of Materials Science and Engineering, Wuhan Institute of Technology, Wuhan, 430074, P. R. China

²Key Laboratory of Marine Materials and Related Technologies, Zhejiang Key Laboratory of Marine Materials and Protective Technologies, Ningbo Institute of Materials Technology and Engineering, Chinese Academy of Sciences, Ningbo 315201, P. R. China.

*E-mail: zhaohaichao@nimte.ac.cn, wangliping@nimte.ac.cn

Received: 2 December 2016 / *Accepted:* 17 February 2017 / *Published:* 12 March 2017

The free amine-containing poly(o-phenylenediamine) (PoPD) nanoparticles with significant dispersibility in organic solvents have been synthesized by chemical oxidative polymerization of o-phenylenediamine mono-hydrochloride salt. The epoxy coatings with different contents of PoPD nanoparticles (0.5 wt%, 1 wt% and 2 wt%) were then prepared by curing reaction of epoxy resin, amine hardener and amine containing PoPD nanoparticles. The corrosion protection properties of the as prepared coatings on Q235 steel were investigated by potentiodynamic polarization, open circuit potential (OCP) and electrochemical impedance spectroscopy (EIS) technique in 3.5 wt % NaCl aqueous solution for 90 days. The results indicate that the coatings with 0.5 wt% PoPD nanoparticles (0.5-PDEP) exhibits high anticorrosive performance, which is attributed to the improved barrier effect of the nano-fillers and redox catalytic capability of embedded PoPD nanoparticles with the evidence of scanning electron microscope (SEM) and XRD. This novel amine-containing PoPD nanoparticles give a promising way to enhance the anticorrosion performance of epoxy coatings and potentially have a wider range of applications in anticorrosion related engineering applications.

Keywords: epoxy; poly (o-phenylenediamine) (PoPD); nanoparticle; Q235; anticorrosion coating

1. INTRODUCTION

Metals and their alloys are widely applied in construction industry, marine, aircraft, cultural heritage and all aspects of life. However, they are highly susceptible to corrosion when exposed to corrosive environments such as soil, humidity, salinity, pH, temperature and biological organisms [1-3]. Meanwhile, corrosion of metals has a huge impact on the economy, which costs more than US\$4

trillion a year equivalent to ~3% of gross domestic product in the worldwide [1]. One of the most efficient way to protect metals against corrosion to is to cover metals with organic coating for isolating them from contacting corrosive environments directly [4]. However, all the organic coatings are not perfect barriers for providing long term corrosion protection for metals because such coatings are more or less permeable to corrosive species such as oxygen, water and ions [5]. Therefore, several mitigation methods and procedures have been developed for organic coating. Some of these control procedures involve adding heavy-metal as corrosion inhibitors [6]. However, heavy metal based corrosion inhibitors usually contain cadmium, chromium, which are highly toxic to the environment and human health [7]. It is therefore important to develop nontoxic, ecofriendly, and effective corrosion inhibitors for retarding the corrosion of metals.

Recent trends in the design of environment-friendly anticorrosive coating have witnessed the utilization of conducting polymers in corrosion protection of oxidizable metals [8]. Especially, polyaniline (PANI) has been a superior candidate for practical applications owing to its excellent anticorrosion properties, ease of synthesis and reversible acid/base doping/dedoping chemistry [9]. Although, the mechanism of protection of metal by PANI is not explored clearly, different mechanistic pathways have been proposed including corrosion inhibitors, shift of electrochemical interface, anodic protection, and barrier protection, etc [10]. Sathiyarayanan et al. investigated the efficient anticorrosion act of phosphate doped polyaniline on the steel in 0.1 N HCl, 0.1 N H₃PO₄ and 3% NaCl [11]. The results confirmed that the oxide layer was stable γ -Fe₂O₃ and α -Fe₂O₃ when iron was coated with PANI containing polymer binder by IR spectroscopy. Chen et al. tested 150 days of polyaniline emeraldine base coating on mild steel in 3.5% NaCl solutions of various pH values, which in combination with the observation of a Fe₂O₃/Fe₃O₄ passive film formed on steel [12]. On the other hand, Kinlen et al. have suggested that Fe-PANI complex is formed in the process of coating steel with PANI. They have believed that the complex's oxidation potential is higher than that of polyaniline, which promotes the reduction of oxygen by a catalytic action [13].

The typical procedure for fabrication of conducting polymer-based anticorrosive coatings can be classified into two different methods, like direct electro-deposition of conducting polymers onto metal substrate, or by incorporation of conducting polymers into organic coating matrix to form composite coatings [10]. Although One can get uniform coating on the metal surfaces by means of electropolymerization, it is a potential issue that corrosion-susceptible metals in the potential domain of the electropolymerization of polyaniline may generate oxidation or dissolution [10]. On the other hand, unsubstituted PANI is only soluble in several high boiling point solvent such as N-methylpyrrolidone (NMP) or dimethylformamide (DMF) [14]. What's more, PANI is nonfusible even by heating up to its decomposition temperature [15]. Hence, the modification of PANI to improve its solubility in organic matrix has to be taken into account. In the literature, the use of PANI nanomaterials as fillers for organic coatings has aroused broad interest in recent years due to their more significant improvement in the corrosion protection properties [16]. Nanostructured polyanilines can act as a bridge interconnecting more molecules and occupy small hole defects formed from local shrinkage during the formulation of coating, thus enhancing the integrity and durability of coatings systems [17, 18]. Huang et al. prepared the poly(o-toluidine)/nano-SiC composite coatings, in which the enhancement of corrosion protection efficiency is due to the formation of more uniformly passive

film on iron surface and the addition of nano-SiC particles increase the tortuosity of the diffusion pathway of corrosive substance [19]. The anti-corrosion behavior of PoPD nanofibers on 316L SS in 3.5% NaCl solution was reported by Muthirulan et al, they found PoPD nanofibers exhibited excellent potential barrier to protect the 316L SS against corrosion in 3.5 % NaCl [20]. Gu et al. had obtained uniform diameters in the range of 60-80 nm of polyaniline/polyvinylpyrrolidone (PANI/PVP) nanoparticles. The addition of 1 wt% PANI/PVP nanoparticles significantly improved the anticorrosion properties of waterborne epoxy coating was measured by polarization curves and EIS tests [21]. Chu et al. had prepared polyaniline nanowires incorporated epoxy resin, which indicated that the coating containing 2 wt% polyaniline nanowires exhibited the highest impedance modulus at 0.01 Hz is close to $1 \times 10^{11} \Omega \text{ cm}^2$ after 60 days of immersion [22].

In the present work, we report the synthesis of poly(o-phenylenediamine) (PoPD) nanoparticles by chemical oxidative polymerization of o-phenylenediamine mono-hydrochloride salt. The obtained nanoparticles exhibit significant dispersibility in organic solvents such as in acetone, THF and ethanol. The epoxy composites coatings (PDEP) with 0.5 wt%, 1 wt% and 2 wt% PoPD were then prepared by curing reaction of epoxy 44, amine hardener and amine containing PoPD nanoparticles. The anticorrosion performance of PDEP on Q235 steel electrode was evaluated through a series of electrochemical corrosion measurements including potentiodynamic polarization, open circuit potential (OCP) and electrochemical impedance spectroscopy (EIS).

2. EXPERIMENTAL

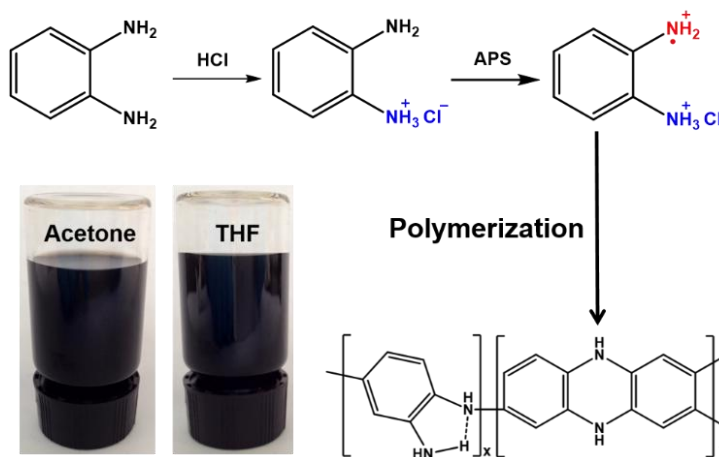
2.1 Materials.

The corrosion studies were conducted on Q235 samples of area 1 cm^2 . Using the EDS method, the chemical composition (in atomic wt%) was given in Table 1. O-phenylenediamine (oPD), ammonium persulfate (APS) and all other solvents were purchased from Aladdin Industrial Corporation. Epoxy resin (E44) and curing agent (polyamide) were purchased from Yunda Chemical Co. Ltd. China. All chemicals and solvent were used as received without further purification.

2.2 Synthesis of soluble PoPD nanoparticles.

The soluble PoPD nanoparticles were synthesized by following procedures [23]: In the first step, o-phenylenediamine (0.55 g, 5 mmol) was dissolved in 0.2 N hydrochloric acid (125 mL) in a beaker and ultrasonicated for 20 min to obtain a homogeneous slight yellow solution. The mixture was cooled to 0~2 °C using an ice bath until the precipitate appeared. Then, the precipitate was separated and washed with diethyl ether to obtain pure mono-hydrochloride salt. In the second step, the 0.58 g mono-hydrochloride salt was dissolved in 100 mL distilled water with magnetic stirring at room temperature for 10 min. Then, APS (1.37 g, 6 mmol) solution in 50 mL ammonia-water solution (20 mL of 20~25% ammonia) was added to above mixture in one portion and the mixture was stirred continuously for 8 h at room temperature. Finally, the solid polymer was filtered and washed with

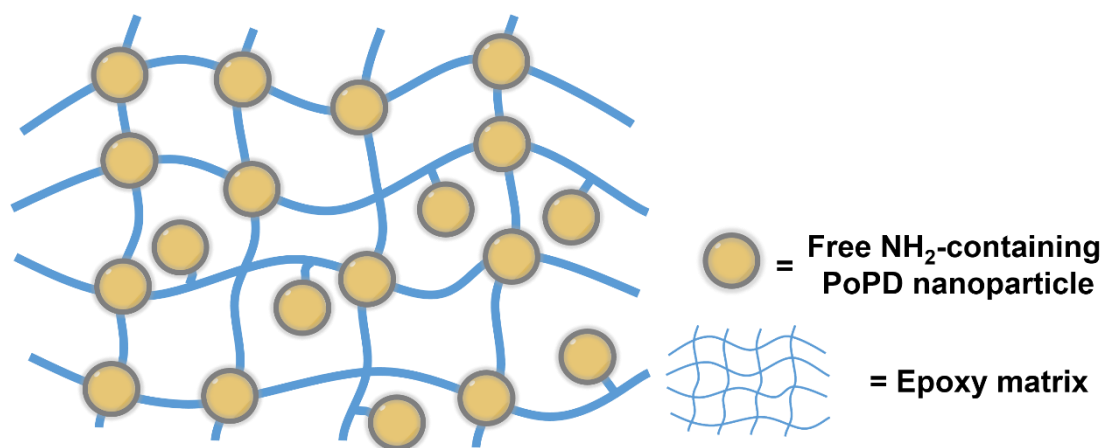
distilled water for several times until the filtrate became colorless. Subsequently the product was dried in a vacuum oven to constant weight.



Scheme 1. Synthetic route for soluble PoPD

2.3 Preparation of PDEP anticorrosion samples.

The pristine Q235 electrode (10 × 10 × 10 mm) was polished with 400, 800 and 1500-grit of sandpapers with automatic polishing machine, then was ultrasonically washed in deionized water and acetone, it was finally dried under nitrogen flow and kept in a desiccator prior to painting.



Scheme 2. Schematic illustration of curing reaction of PoPD nanoparticles in epoxy matrix.

Scheme 2 shows the proposed curing procedures of PDEP samples. A certain amount of PoPD nanoparticles was dissolved in ethanol and sonicated for 0.5 h to obtain a homogenous solution. A precalculated E44 epoxy was added to the above solution and carefully stirred for 0.5 h, then the ethanol was removed by rotary evaporating. Afterward, the stoichiometric amount of polyamide (25 wt% of E44 epoxy) curing agent was added in polymer matrix. The mixture was stirred thoroughly with high speed blender (PI7500 R75G1, POWTRAN) at 4000 rpm for 5 min after it was degassed in a

vacuum oven to remove the trapped air bubbles. Finally, the degassed mixture was poured onto Q235 electrode with a wire bar coater, and the samples were cured at room temperature for 3 days. The pure epoxy as comparison was prepared by the same procedure without PoPD nanoparticles. PDEP samples with various PoPD contents (0~2 wt % relative to the whole quality) as denoted the neat epoxy, 0.5-PDEP, 1-PDEP and 2-PDEP. The coating thickness was $20 \pm 5 \mu\text{m}$ measured using a PosiTector6000FNS1 apparatus.

2.4 Characterization.

Fourier transform infrared (FT-IR) spectra was obtained on NICOLET 6700 spectrometer. UV-vis spectrum was recorded between 230 and 800 nm using Lambda 950 spectroscope. The Raman spectra were measured by Renishaw inVia Reflex at the wavelength of 632.8 nm. X-ray powder diffraction (XRD) patterns were obtained with D8 ADVANCE diffractometer using Cu K α radiation at the scan range of 2θ from 10° to 80° . The scanning electron microscope (SEM) images of PoPD nanoparticles and the section of coating were taken by HITACHI S4800. The corrosion products formed on the Q235 substrates were characterized by SEM (EDS) and XRD. The scans of XRD measurement were performed in a 2θ range of $10\sim 90^\circ$ with a scan speed of $0.09^\circ (2\theta)/\text{s}$. All major XRD peaks were assigned to the compounds listed in the PDF cards.

The electrochemical corrosion test was conducted in 3.5 wt % NaCl solution on CHI-660E electrochemical workstation, with Pt plate and saturated calomel electrode (SCE) as counter electrode and reference electrode, respectively. The corrosion potential (E_{corr}) of the coating/Q235 steel working electrode was obtained from the open circuit potential at the balance state of the system. For EIS measurement was carried out in the frequency range of 10^5 to 0.01 Hz. Corrosion parameters from EIS data were fitted by using ZsimpWin software. Polarization curves were performed with 0.2 mV/s scan rate and started from a potential of -500 mV to +500 mV vs OCP.

3. RESULTS AND DISCUSSION

3.1 Characterization of soluble PoPD nanoparticles.

FTIR spectra was used to characterize the functional groups of the synthesized PoPD nanoparticles, which is presented in Figure 1a. A broad band is appeared in the region 3225 cm^{-1} due to the stretching of hydrogen bonded $-\text{NH}_2$, and/or $-\text{NH}-$ groups in the polymer. The other main peaks located at 1620, 1502 and at 1290, 1116 cm^{-1} correspond to the stretching vibrations of quinoid C-C, benzenoid C-C and quinoid C-N, benzenoid C-N bonds, respectively [24]. UV-vis spectroscopy is used to confirm the conjugated structure of PoPD, as shown in Figure 1b. The PoPD nanoparticles show two absorption peaks at 290 and 423 nm in UV-vis region [25]. The absorption spectrum around 290 nm indicates $\pi-\pi^*$ transition associated with the phenazine unit conjugated to long pairs of bridging nitrogens. The absorption observed at 423 nm is attribute to excitonic transition in quinoid-imine units. Figure 1c shows Raman spectrum of PoPD nanoparticles. Obviously, there is a peak at 1153 cm^{-1} attributed to the C-H in-plane bending mode in the presence of quinoid ring. C-N

stretching mode of polaronic units appear at 1242 cm^{-1} , which is a weak band. The Raman spectrum also reveals that the peaks located between 1345 and 1393 cm^{-1} are assigned to the C-N^+ stretching modes of the delocalized polaronic charge carriers [25]. What's more, N-H bending deformation mode is situated at 1535 cm^{-1} . Only a broad characteristic peak of XRD pattern appeared at $2\theta = 21^\circ$, indicating the amorphous nature of the conducting polymer (Figure 1d) [26]. Figure 2 presents the typical SEM images of PoPD nanoparticles. It is noted that the uniform PoPD solid nanoparticles with a diameter of ca. 100 nm were successfully obtained.

Table 1. Chemical composition (wt %) of the Q235 used.

B	C	O	Si	Cr	Mn	Fe
0.58	5.62	0.48	0.20	0.02	0.41	Bal.

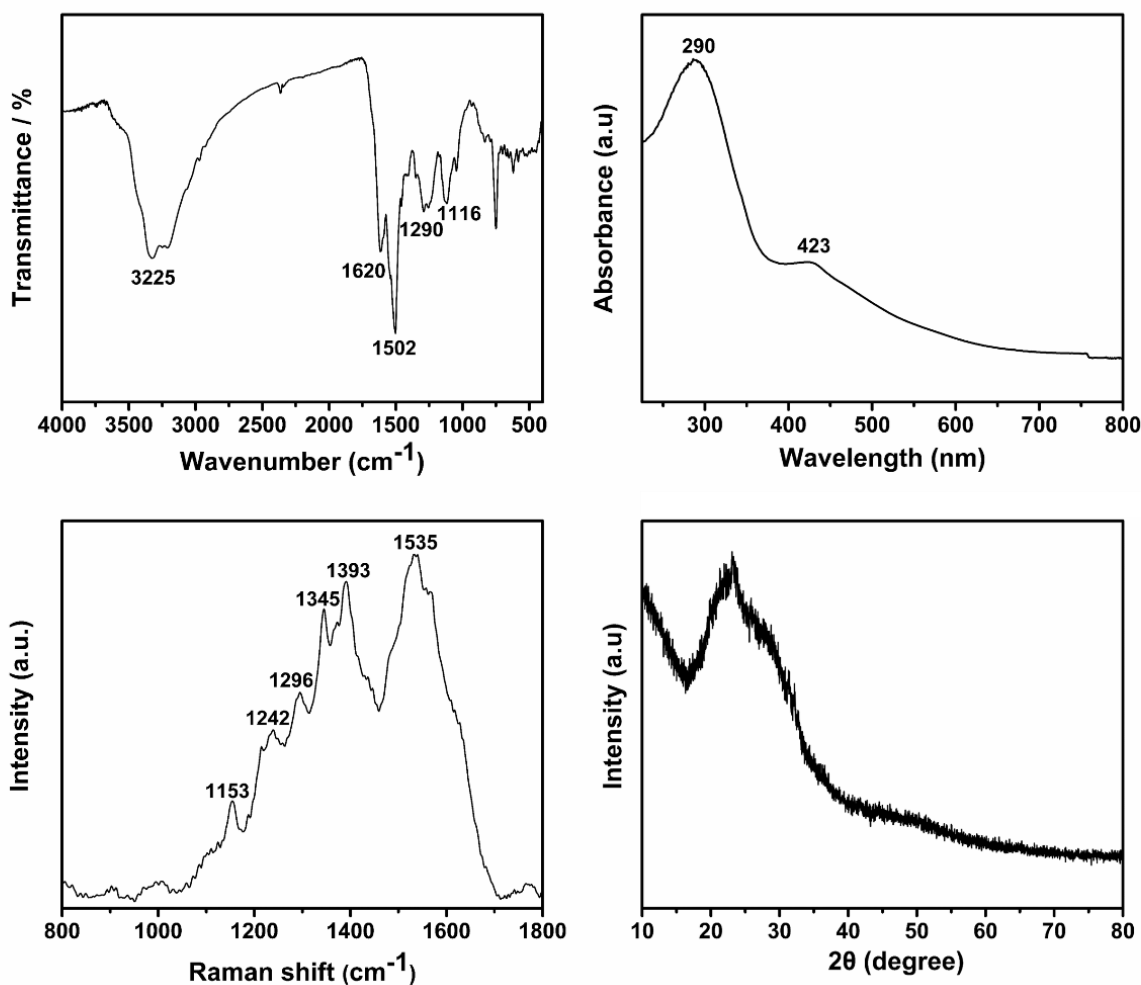


Figure 1. (a) FTIR, (b) UV-vis, (c) Raman spectrum and (d) XRD pattern of soluble PoPD.

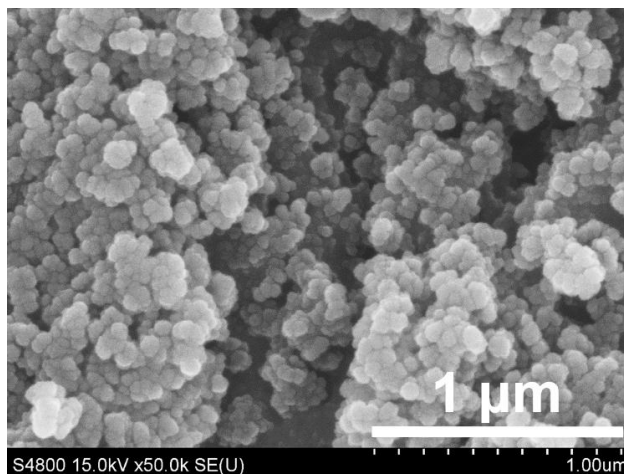


Figure 2. Typical SEM image of PoPD nanoparticles

3.2 Morphology of PDEP coatings

To investigate the dispersion capability of PoPD nanoparticles in the epoxy matrix, the morphologies of PDEP coatings and neat epoxy were observed by SEM. The fracture surface of neat epoxy exhibits typical bamboo-like surface and an oriented brittle fracture patterns initialized from the cracks. The area between the oriented cracks is very smooth, due to rapid crack propagation. By addition of PoPD nanoparticles, the cross-section of PDEP coating is coarse and fracture cracks propagation is disturbed. As shown in Figure 3b, with the less amount of the PoPD nanoparticles (0.5 wt %), it can obtain a highly disperse PDEP.

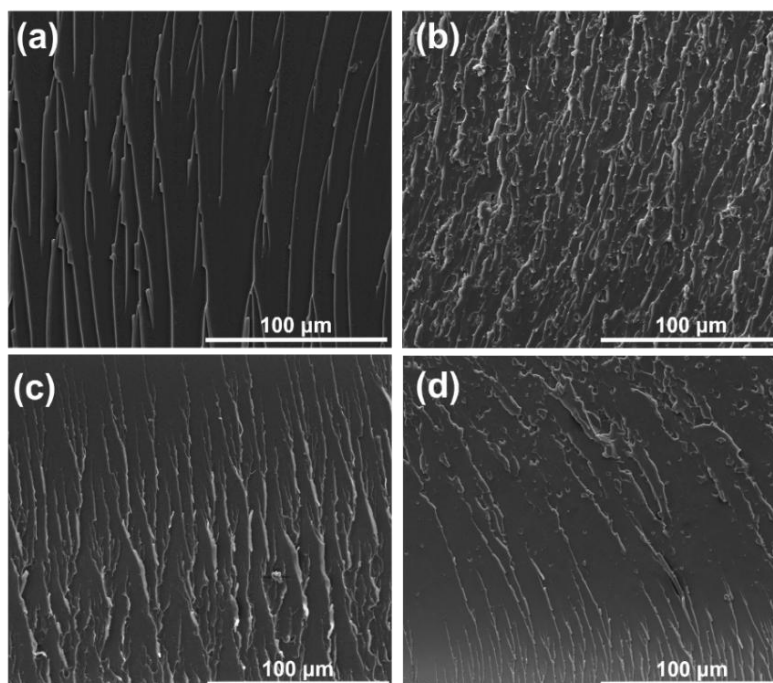


Figure 3. Typical SEM images of cross-section from (a) neat epoxy, (b) 0.5-PDEP, (c) 1-PDEP, (d) 2-PDEP.

3.3 Electrochemical analysis

The corrosion performance of as prepared coatings was evaluated by potentiodynamic polarization curves, open circuit potential (OCP), electrochemical impedance spectroscopy (EIS) measurements, respectively. All the electrochemical measurements were conducted with 3 replicates, and the representative results are discussed in the following.

Figure 4 displays the Tafel plots for neat epoxy, 0.5-PDEP, 1-PDEP and 2-PDEP composite coated steel samples and uncoated steel in 3.5 wt % NaCl solution under potentiodynamic polarization conditions after 90 days of immersion. The corrosion protection of the synthesized PoPD nanoparticles coated steel can be observed from the values of the corrosion potential (E_{corr}), corrosion current (i_{corr}) as listed in Table 2. Generally, a higher E_{corr} value represents a good anticorrosion property of the coating and a lower i_{corr} value indicates slow corrosion rate [27]. As seen from the Tafel plots, the coated polymer coatings possess a larger positive E_{corr} than the bare Q235, which reveals the obvious protection from the polymer coatings. The E_{corr} values of 0.5-PDEP, 1-PDEP and 2-PDEP are -0.347, -0.426, -0.569 V, respectively. With the increase PoPD content, the E_{corr} gradually decrease. i_{corr} was obtained through extrapolation of the straight line along the linear portion of the anodic and cathodic polarization curves to the E_{corr} axis to obtain the intersection point. Polarization resistance (R_p) was calculated by applying the following Stern–Geary equation [27]:

$$R_p = \frac{k_a k_b}{2.303(k_a + k_b)i_{corr}} \quad (1)$$

where i_{corr} is the corrosion current ($\mu\text{A}/\text{cm}^2$), which was determined via the intersection of the anodic and cathodic lines and k_a and k_b ($\Delta E/\Delta \log i_{corr}$) are the anodic and cathodic slopes, respectively. The corrosion rate (CR, mm/year) was calculated to analyze the anticorrosion performance of the coatings quantitatively. The corrosion rate (CR) was calculated using the following formula [10]:

$$CR = \frac{kM \cdot i_{corr}}{\rho_m} \quad (2)$$

where i_{corr} is the corrosion current (A/cm^2), k is a constant ($3268.6 \text{ mol}/\text{A}$), M is the molecular weight of Fe ($56 \text{ g}/\text{mol}$), and ρ_m is the density ($7.85 \text{ g}/\text{cm}^3$).

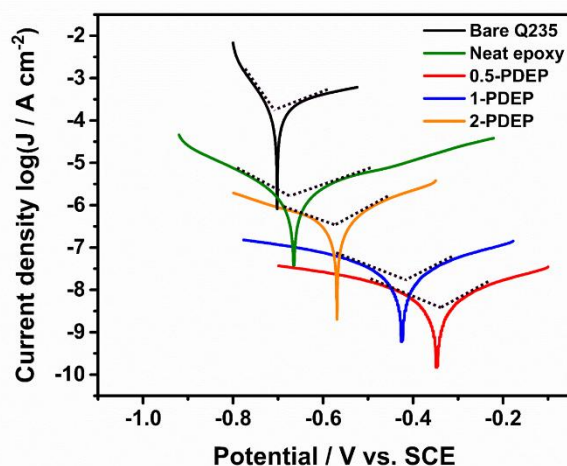


Figure 4. Tafel plots for different coatings after immersion in 3.5 wt % NaCl aqueous solution for 90 days.

It is well known that the cathodic and anodic of corrosion process could be separated by the PoPD nanoparticles and the cathodic reaction was changed to be the reaction between the PoPD nanoparticles. As compared to cathodic Tafel slope (β_c), the higher values of β_a for the coated steel indicated that the application of external current strongly polarized the anode. The development of PoPD nanoparticles containing coating on the steel surface highly influenced the k_a values, as a consequence of which the anodic dissolution was decelerated [10, 18]. As shown in Table 2, the neat epoxy coated Q235 only has a low R_p value of $0.797 \text{ k}\Omega \text{ cm}^2$ after 90 days of immersion. Such lower value of polarization resistance (R_p) implied that the coating can't afford good barrier to resist the corrosion [19]. When pure epoxy coating is immersed in saline media, corrosion-assisting small molecules, such as O_2 and H_2O or ions (Na^+ , Cl^-) can easily penetrate into the epoxy film and directly contact with the steel surface, so corrosion takes place immediately [28]. While adding excessive amounts of PoPD nanoparticles, polarization resistances negatively shift, and the corrosion rate gradually increase. As 0.5-PDEP have maintained to a high value as $190 \text{ k}\Omega \text{ cm}^2$ after 90 days of immersion in saline media, indicating better corrosion protection than other coatings.

Table 2. Electrochemical parameters calculated from the potentiodynamic polarization curves of anticorrosion coatings in 3.5 wt% NaCl solution.

Samples	E_{corr} (V)	i_{corr} ($\mu\text{A}/\text{cm}^2$)	β_a (mV dec^{-1})	β_c (mV dec^{-1})	R_p ($\text{K}\Omega \cdot \text{cm}^2$)	CR (mm/year)
Bare Q235	-0.702	10.15	67.13	327.3	2.38	0.237
Neat epoxy	-0.664	1.506	206.3	190.4	25.58	0.035
0.5-PDEP	-0.347	5.375×10^{-3}	217.3	155.7	8.2×10^3	1.25×10^{-4}
1-PDEP	-0.426	6.395×10^{-2}	208.5	205.6	702.7	1.49×10^{-3}
2-PDEP	-0.569	5.185×10^{-1}	182.4	304.9	95.58	1.21×10^{-2}

The variation of OCP with time for the as prepared coatings in 3.5% NaCl is shown in Figure 5. The initial OCP values of the pure epoxy coated steel is -0.464 V vs SCE. After 90 days of exposure to 3.5 wt % NaCl solution, the OCP value of the pure epoxy gradually decrease to -0.698 V SCE. Initially, the OCP value of the 0.5-PDEP coated steel is about -0.04 V vs SCE while those of the 1-PDEP and 2-PDEP coated steel are -0.211 and -0.195 V vs SCE, respectively. The OCP values of all the samples containing PoPD nanoparticles are shifted to noble region after 12 days of immersion, indicating that PoPD nanoparticles in the coatings are able to passivate the iron surface in 3.5 wt % NaCl media [10]. It also can be observed that the 0.5-PDEP exhibits higher OCP value than those of the 1-PDEP and 2-PDEP coated steel. In fact, for 0.5-PDEP, the OCP remains at -0.31 V vs SCE even after 90 days of exposure to saline solution, demonstrating the best anticorrosive performance.

EIS is used to investigate the protective nature of the coatings by measuring the coatings resistance (R_c) and the coatings capacitance (Q_c) of the coatings [29]. Coatings with high resistance values ($>1 \times 10^7 \Omega \text{ cm}^2$) and low capacitance values ($<1 \times 10^{-9} \text{ F cm}^2$) have been found to offer

corrosion protection of steel [30]. Impedance plots (Bode plots, impedance versus frequency) of the neat epoxy, 0.5-PDEP, 1-PDEP and 2-PDEP coated Q235 steel after 90 days of immersion in 3.5% NaCl solution are shown in Figure 6. Usually, the impedance modulus at the lowest frequency ($Z_{f=0.01\text{Hz}}$) in Bode plot could be used as a semi-quantitative indicator of coating's barrier performance. The Bode-modulus plots of neat epoxy show a high $Z_{f=0.01\text{ Hz}}$ value ($1.11 \times 10^{10} \Omega \text{ cm}^2$) at the onset of immersion (Figure 6a₁). Even that initial value of neat epoxy is higher than other three coatings. However, the $Z_{f=0.01\text{ Hz}}$ value of neat epoxy gradually decrease to $3.97 \times 10^5 \Omega \text{ cm}^2$ after 90 days of immersion, which indicates small molecules (H_2O and O_2 or ions) could easily penetrate epoxy coating and degrades substrate. While for all the epoxy coatings containing PoPD nanoparticles, $Z_{f=0.01\text{ Hz}}$ of PDEP can be maintained at relatively high values after 90 days of immersion, indicating the better corrosion protection. For the specific impedance behavior of 0.5-PDEP, 1-PDEP and 2-PDEP. The $Z_{f=0.01\text{ Hz}}$ values of 1-PDEP and 2-PDEP are found to decrease from $1.27 \times 10^9 \Omega \text{ cm}^2$ and $7.76 \times 10^8 \Omega \text{ cm}^2$ at the onset of immersion to $1.38 \times 10^8 \Omega \text{ cm}^2$ and $1.81 \times 10^7 \Omega \text{ cm}^2$ after 60 days of immersion. Afterward, the $Z_{f=0.01\text{ Hz}}$ values of two coatings increase to 1.74×10^8 and $2.33 \times 10^7 \Omega \text{ cm}^2$ after 70 days and reach 2.43×10^7 and $7.15 \times 10^6 \Omega \text{ cm}^2$ after 90 days of immersion. Initially 0.5-PDEP has a $Z_{f=0.01\text{ Hz}}$ value of $5.94 \times 10^9 \Omega \text{ cm}^2$ that increases to $4.31 \times 10^{10} \Omega \text{ cm}^2$ after 6 days of immersion, then the $Z_{f=0.01\text{ Hz}}$ value decreases to $4.21 \times 10^8 \Omega \text{ cm}^2$ after 60 days of immersion. There is a weak gain in $Z_{f=0.01\text{ Hz}}$ value of $1.24 \times 10^9 \Omega \text{ cm}^2$ after 70 days, and it reach $7.25 \times 10^7 \Omega \text{ cm}^2$ after 90 days of immersion. All three PDEP coatings, the increased $Z_{f=0.01\text{ Hz}}$ values after an initial decrease can be attributed to the passivation effect of PoPD nanoparticles [22]. Also, it is observed that 0.5-PDEP always maintained the shape of two-time constant capacitive loops (Figure 6d₁). Moreover, the long-term anticorrosion performance of 0.5-PDEP could also be reflected by the high phase angles ($\sim 83^\circ$) during the whole immersion period (Figure 6d₃).

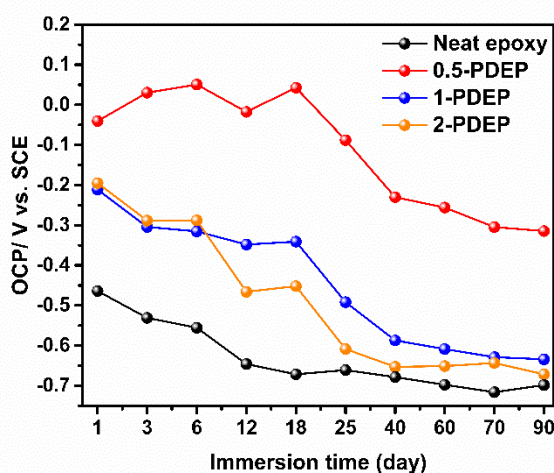


Figure 5. Open circuit potential of different coatings during the immersion of 90 days in 3.5 wt % NaCl solution

The EIS results are further fitted by ZsimpWin software using the equivalent electric circuits shown in Figure 7, where R_s is the solution resistance, R_c and Q_c denote coating resistance and coating capacitance, respectively. Q_{dl} represents a double-layer capacitance and R_{ct} is a charge transfer

resistance [27]. The fitting results are shown in Figure 7b. It can be seen that the R_c of neat epoxy gradually decreases from $1.02 \times 10^{10} \Omega \text{ cm}^2$ to a much lower value ($2.86 \times 10^5 \Omega \text{ cm}^2$). The R_c values of 1-PDEP and 2-PDEP decrease to 1.97×10^7 and $6.76 \times 10^6 \Omega \text{ cm}^2$, while the 0.5-PDEP coating is one or two order of magnitude higher than 1-PDEP and 2-PDEP after the immersion of 90 days. The R_c indicates the decrease in corrosion protection ability of the coating. Consequently, it is observed that 0.5-PDEP exhibited the outstanding corrosion resistance, which was consistent with the potentiodynamic polarization results. From the above results, we can conclude that the well-dispersed nanoparticles in the epoxy matrix enhance shielding function and also increase the tortuosity of diffusion pathway of H_2O , O_2 and electrolyte [32, 33]. This multifunction effect leads to the excellent anticorrosion performance of 0.5-PDEP coatings.

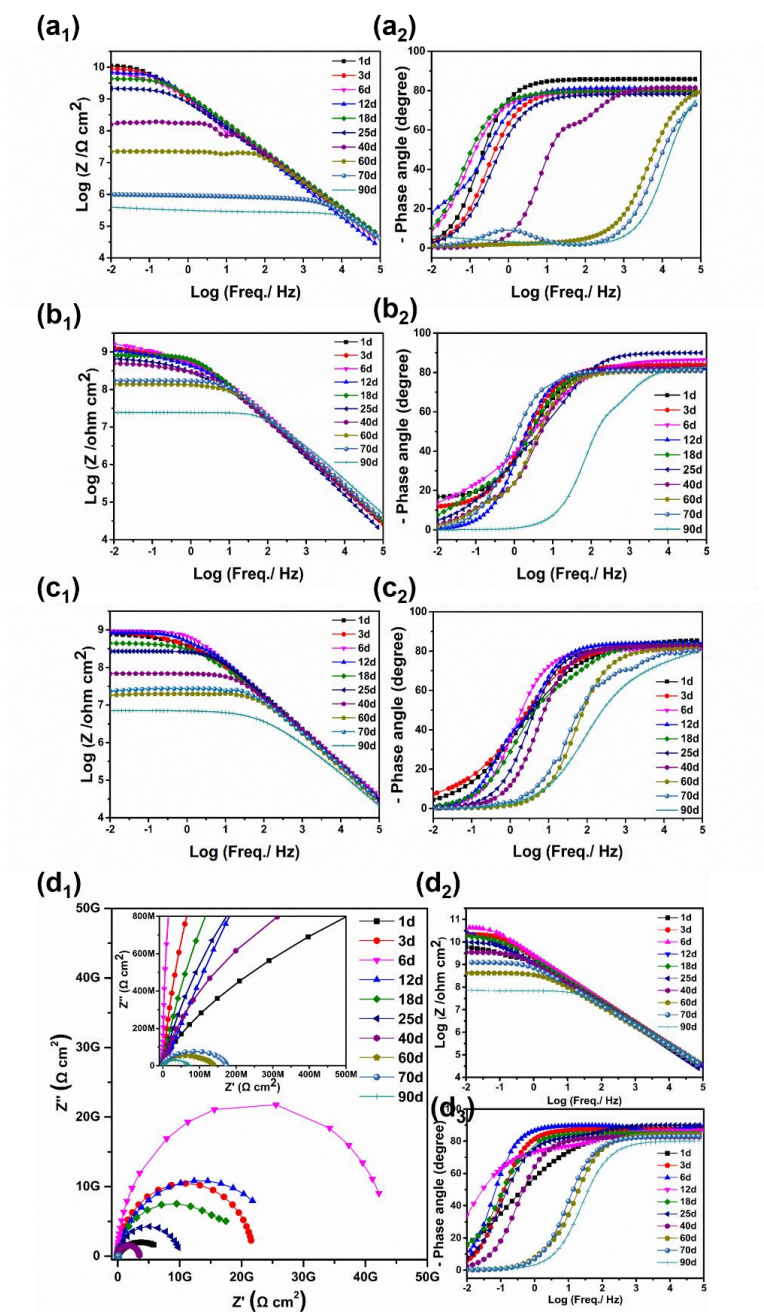


Figure 6. Nyquist plots of (d₁) 0.5-PDEP and Bode plots of (a₁) (a₂) neat epoxy, (b₁) (b₂) 1-PDEP, (c₁) (c₂) 2-PDEP, (d₂) (d₃) 0.5-PDEP during 90 days of immersion in 3.5 wt% NaCl solution.

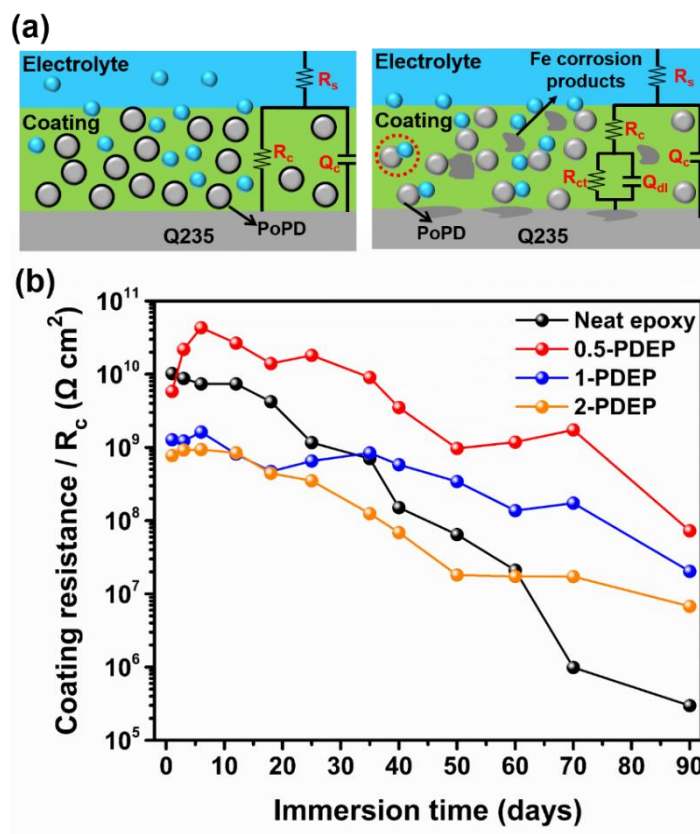


Figure 7. (a) Equivalent electric circuits and (b) the fitting results of the collected EIS results of different coatings as a function of immersion time.

3.4 Surface Characterization

The morphology of metal surface underneath the organic coatings after 90 day of immersion is shown in Figure 8. There are smaller scale of corrosive region and the nearly invisible polishing grooves (Figure 8b). The fresh compact layer of uniform microstructure is developed on the substrate, which has improved the corrosion resistance of the material. With higher content of PoPD nanoparticles in epoxy blend (Figure 8c, d), the interface appears as porous morphology. Meanwhile, cracks with the structure of corrosion products like “honeycomb” are developed on the metal surface [18]. However, it can also be seen that the morphology of neat epoxy coated steel shows a smooth film covered with mushroom like products after 90 days of exposure to saline environment (Figure 8a). The corresponding EDS tests (Figure 9) show that obvious chlorides are found on underlying surface covered for pure epoxy coating, and Na ions are appeared in the corrosion products of PDEP coatings [34].

XRD patterns were employed to further analyze the corrosion product of metal surface after the coatings were peeled off after 90 days of immersion in 3.5% NaCl. The metal surface underneath pure epoxy coating exhibits a strong characteristic peak attributed to β -FeOOH because chlorides facilitate the formation of rust (Figure 10) [35]. For the coatings containing PoPD nanoparticles, it is shown that the formation of β -FeOOH is suppressed, and the formation of obvious inert protective layer, i.e. Fe_2O_3

and Fe₃O₄, are observed [36, 37]. The conducting PoPD nanoparticles facilitate the formation of passive oxide on the steel surface and retard the aggressive anions such as chloride, water and oxygen from penetrating through the coating to the substrate.

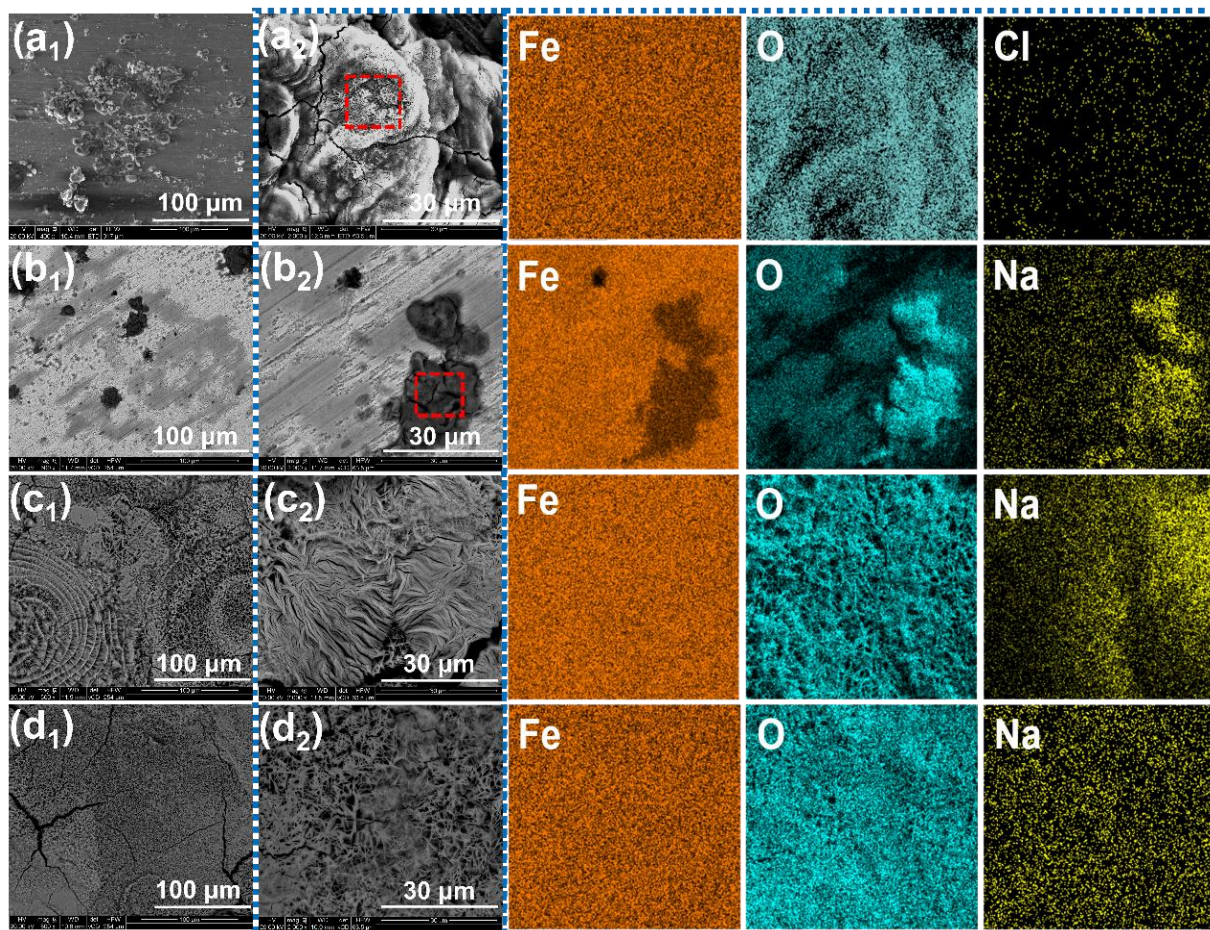


Figure 8. SEM images of corrosion products on the steel substrate coated by (a₁, a₂) neat epoxy, (b₁, b₂) 0.5-PDEP, (c₁, c₂) 1-PDEP and (d₁, d₂) 2-PDEP after 90 days of immersion. The EDS was given by blue box.

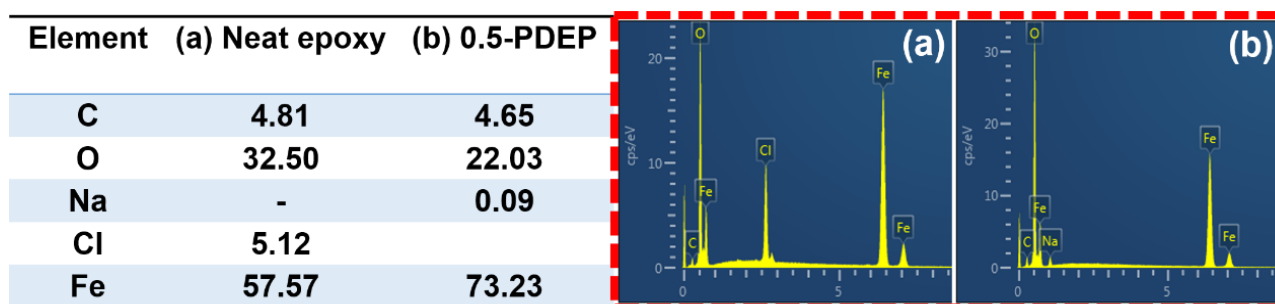


Figure 9. EDS data (wt.% of each element) obtained from the imaged red areas in Figure8 a₂ and b₂ are presented in (a) and (b).

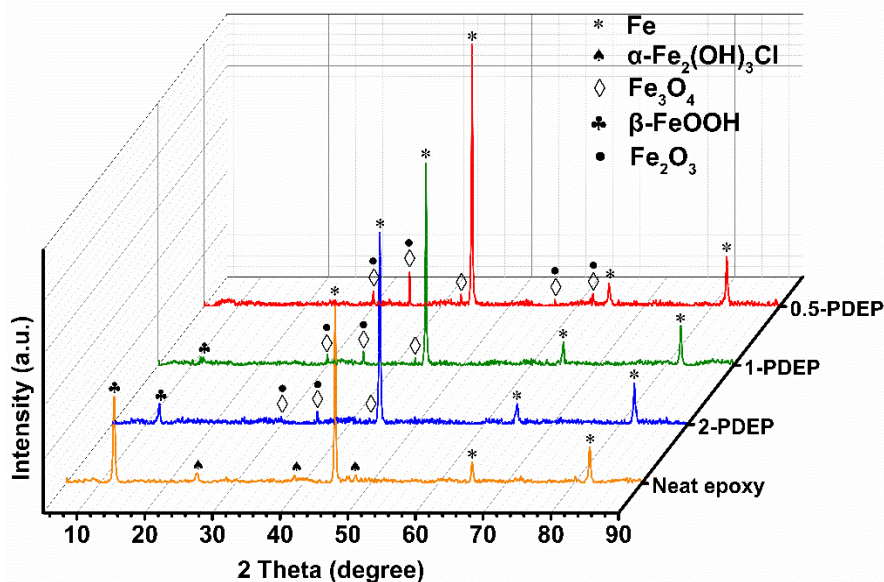


Figure 10. XRD patterns of surface of Q235 coated by different coatings after 90 days of exposure to 3.5% NaCl solution.

4. CONCLUSIONS

The amine-containing PoPD nanoparticles with enhanced solubility and reactivity were fabricated via a facile chemical oxidative polymerization approach, and the epoxy coatings containing 0.5 wt%, 1 wt%, and 2 wt% PoPD nanoparticles were successfully prepared by curing reaction of epoxy resin, amine hardener, and amine contain PoPD nanoparticles. The corrosion behavior of the coatings on Q235 immersed in the 3.5 wt % NaCl solution was investigated by potentiodynamic polarization, the OCP versus time of exposure and EIS measurements. The results demonstrated that 0.5-PDEP was able to offer the best corrosion protection, which was attributed to the formation of effective Fe₂O₃ and Fe₃O₄ passive layer distributed on the carbon steel surface evidenced by SEM and XRD analysis. This novel amine-containing PoPD nanoparticles give a promising way to enhance the anticorrosion performance of epoxy coatings and potentially have a wider range of applications in anticorrosion related engineering applications.

ACKNOWLEDGEMENTS

The authors gratefully appreciate financial support provided by Zhejiang Provincial Natural Science Fund (LY16B040004), One Hundred Talented People of the Chinese Academy of Sciences (Y60707WR04).

References

1. X. Li, D. Zhang, Z. Liu, Z. Li, C. Du, C. Dong, *Nature*, 527 (2015) 441.
2. A. Solé, L. Miró, C. Barreneche, I. Martorell, L. F. Cabeza, *Renew. Energ.*, 75 (2015) 519.

3. X. F. Zhang, R. J. Chen, Y. H. Liu, J. M. Hu, *J. Mater. Chem. A*, 4 (2015) 649.
4. F. Meng, L. Liu, W. Tian, H. Wu, Y. Li, T. Zhang, F. Wang, *Corros. Sci.*, 101 (2015) 139.
5. H. Wei, Y. Wang, J. Guo, N. Z. Shen, D. Jiang, X. Zhang, X. Yan, J. Zhu, Q. Wang, L. Shao, *J. Mater. Chem.*, 3 (2015) 469.
6. A. Stankiewicz, Z. Jagoda, K. Zielińska, I. Szczygieł, *Mater. Corros.*, 66 (2015) 1391.
7. U. Eduok, R. Suleiman, J. Gittens, M. Khaled, T. J. Smith, R. Akid, B. El Ali, A. Khalil, *RSC Adv.*, 5 (2015) 93818.
8. P. P. Deshpande, N. G. Jadhav, V. J. Gelling, D. Sazou, *J. Coat. Technol. Res.*, 11 (2014) 473.
9. W. P. Hou, Y. Liu, Z. Y. Ge, W. Y. Zhao, *Mater. Corros.*, 64 (2013) 960.
10. N. Sarkar, G. Sahoo, R. Das, G. Prusty, D. Sahu, S. K. Swain, *Ind. Eng. Chem. Res.*, 55 (2016) 2921.
11. S. Sathiyarayanan, S. Muthkrishnan, G. Venkatachari, *Electrochim. Acta*, 51 (2006) 6313.
12. Y. Chen, X. H. Wang, J. Li, J. L. Lu, F. S. Wang, *Corros. Sci.*, 49 (2007) 3052.
13. P. J. Kinlen, D. C. Silverman, C. R. Jeffreys, *Synthetic Met.*, 85 (1997) 1327.
14. D. Ichinohe, T. Aral, H. Kise, *Synthetic Met.*, 84 (1997) 75.
15. C. Xing, Z. Zhang, L. Yu, G. I. Waterhouse, L. Zhang, *Prog. Org. Coat.*, 77 (2014) 354.
16. S. Zhao, Z. Wang, X. Wei, B. Zhao, J. Wang, S. Yang, S. Wang, *Ind. Eng. Chem. Res.*, 51 (2012) 4661.
17. R. Yuan, S. Wu, B. Wang, Z. Liu, L. Mu, T. Ji, L. Chen, B. Liu, H. Wang, J. Zhu, *Polymer*, (2016).
18. J. Ding, H. Zhao, L. Gu, S. Su, H. Yu, *Int. J. Electrochem. Sci.*, 11 (2016) 7066.
19. J. Huang, C. Hu, Y. Qing, *Int. J. Electrochem. Sci.*, 10 (2015) 10607.
20. P. Muthirulan, N. Kannan, M. Meenakshisundaram, *J. Adv. Res.*, 4 (2013) 385.
21. L. Gu, X. Zhao, X. Tong, J. Ma, B. Chen, S. Liu, H. C. Zhao, H. B. Yu, J. M. Chen, *Int. J. Electrochem. Sci.*, 11 (2016) 1621.
22. D. Chu, J. Wang, Y. Han, Q. Ma, Z. Wang, *RSC Adv.*, 5 (2015) 11378.
23. S. Samanta, P. Roy, P. Kar, *Macromol. Res.*, 24 (2016) 342.
24. U. Olgun, M. Gülfen, *React. Funct. Polym.*, 77 (2014) 23.
25. J. F. Feng, T. Sun, J. Zhu, *Synthetic Met.*, 213 (2016) 12.
26. C. Yuan, X. Liu, M. Jia, Z. Luo, J. Yao, *J. Mater. Chem.*, 3 (2014) 3409.
27. B. Grgur, A. Elkais, M. Gvozdenović, S. Drmanić, T. L. Trišović, B. Jugović, *Prog. Org. Coat.*, 79 (2015) 17.
28. C. Hu, Y. Zheng, Y. Qing, F. Wang, C. Mo, Q. Mo, *J. Inorg. Organomet. Poly. Mater.*, 25 (2015) 583.
29. X. Sheng, W. Cai, L. Zhong, D. Xie, X. Zhang, *Ind. Eng. Chem. Res.*, 55 (2016) 8576.
30. E. Husain, T. N. Narayanan, J. J. Tijerina, S. Vinod, R. Vajtai, P. M. Ajayan, *ACS Appl. Mater. Interfaces*, 5 (2013) 4129.
31. J. D. Scantlebury, K. Galić, *Prog. Org. Coat.*, 31 (1997) 201.
32. A. Ganash, *J. Nanomater.*, 2014 (2014) 1.
33. L. A. Juhaiman, D. A. Al-Enezi, W. K. Mekhamer, *Int. J. Electrochem. Sci.*, 11 (2016) 5618.
34. S. Jafarzadeh, P. M. Claesson, P.E. Sundell, E. Tyrode, J. Pan, *Prog. Org. Coat.*, 90 (2016) 154.
35. S. Li, R. D. George, L. Hihara, *Corros. Sci.*, 102 (2016) 36.
36. S. Pour-Ali, C. Dehghanian, A. Kosari, *Corros. Sci.*, 85 (2014) 204.
37. C. Chen, S. Qiu, M. Cui, S. Qin, G. Yan, H. Zhao, L. Wang, Q. Xue, *Carbon*, 114 (2017) 356.